Imaging of CO_2 bubble plumes above an erupting submarine volcano, NW Rota-1, Mariana Arc

Citation	Chadwick Jr., W. W., Merle, S. G., Buck, N. J., Lavelle, J. W., Resing, J. A., & Ferrini, V. (2014). Imaging of CO_2 bubble plumes above an erupting submarine volcano, NW Rota-1, Mariana Arc. Geochemistry Geophysics Geosystems, 15 (11), 4325-4342. doi:10.1002/2014GC005543
DOI	10.1002/2014GC005543
Publisher	American Geophysical Union
Version	Version of Record
Terms of Use	http://cdss.library.oregonstate.edu/sa-termsofuse

AGU PUBLICATIONS

Geochemistry, Geophysics, Geosystems

RESEARCH ARTICLE
10.1002/2014GC005543

Special Section:
Assessing Magmatic, Neovolcanic, Hydrothermal, and Biological Processes along Intra-Oceanic Arcs and Back-Arcs

Imaging of CO_2 bubble plumes above an erupting submarine volcano, NW Rota-1, Mariana Arc

William W. Chadwick Jr.[1], Susan G. Merle[1], Nathaniel J. Buck[2], J. William Lavelle[3], Joseph A. Resing[2], and Vicki Ferrini[4]

[1]Cooperative Institute for Marine Resources Studies, Oregon State University, Newport, Oregon, USA, [2]Joint Institute for the Study of the Atmosphere and Ocean, University of Washington, Seattle, Washington, USA, [3]NOAA, Pacific Marine Environmental Laboratory, Seattle, Washington, USA, [4]Lamont-Doherty Earth Observatory, Columbia University, Palisades, New York, USA

Key Points:
- CO_2 bubble plumes were imaged by multibeam sonar at actively erupting NW Rota-1
- The bubble plumes reflected the variable style and vigor of eruptive activity
- The height and shape of the bubble plumes varied in concert with ocean currents

Supporting Information:
- Readme
- Movies ms01–ms11

Correspondence to:
W. W. Chadwick Jr.,
bill.chadwick@oregonstate.edu

Citation:
Chadwick Jr., W. W., S. G. Merle, N. J. Buck, J. W. Lavelle, J. A. Resing, and V. Ferrini (2014), Imaging of CO_2 bubble plumes above an erupting submarine volcano, NW Rota-1, Mariana Arc, *Geochem. Geophys. Geosyst.*, *15*, 4325–4342, doi:10.1002/2014GC005543.

Received 15 AUG 2014
Accepted 27 OCT 2014
Accepted article online 30 OCT 2014
Published online 25 NOV 2014

Abstract NW Rota-1 is a submarine volcano in the Mariana volcanic arc located ~100 km north of Guam. Underwater explosive eruptions driven by magmatic gases were first witnessed there in 2004 and continued until at least 2010. During a March 2010 expedition, visual observations documented continuous but variable eruptive activity at multiple vents at ~560 m depth. Some vents released CO_2 bubbles passively and continuously, while others released CO_2 during stronger but intermittent explosive bursts. Plumes of CO_2 bubbles in the water column over the volcano were imaged by an EM122 (12 kHz) multibeam sonar system. Throughout the 2010 expedition numerous passes were made over the eruptive vents with the ship to document the temporal variability of the bubble plumes and relate them to the eruptive activity on the seafloor, as recorded by an in situ hydrophone and visual observations. Analysis of the EM122 midwater data set shows: (1) bubble plumes were present on every pass over the summit and they rose 200–400 m above the vents but dissolved before they reached the ocean surface, (2) bubble plume deflection direction and distance correlate well with ocean current direction and velocity determined from the ship's acoustic doppler current profiler, (3) bubble plume heights and volumes were variable over time and correlate with eruptive intensity as measured by the in situ hydrophone. This study shows that midwater multibeam sonar data can be used to characterize the level of eruptive activity and its temporal variability at a shallow submarine volcano with robust CO_2 output.

1. Introduction

The newest generation of multibeam sonar systems, commonly used on research vessels for seafloor mapping, can also record acoustic backscatter data in the water column. This capability can be used to image plumes of bubbles rising from the seafloor, because gas bubbles are good reflectors of acoustic energy due to the large difference in sound speed and density between water and gas and resonance effects controlled by bubble size, sonar frequency, and water depth [*Medwin and Clay*, 1998; *Weber et al.*, 2014]. Single-beam echo sounders have also been used to study aqueous bubble plumes [*Cardigos et al.*, 2005; *Greinert et al.*, 2006; *Sauter et al.*, 2006; *Westbrook et al.*, 2009; *Leifer et al.*, 2010; *Caudron et al.*, 2012; *Kannberg et al.*, 2013], but multibeam sonars allow wider coverage, higher resolution, and three-dimensional spatial information. Previous studies using multibeam sonars have generally been conducted in continental margin settings where hydrocarbon seeps of methane gas bubbles are found [*Schneider von Deimling et al.*, 2007; *Greinert*, 2008; *Gardner*, 2009; *Greinert et al.*, 2010; *Schneider von Deimling et al.*, 2010, 2011; *Weber et al.*, 2014]. Although some previous single-beam investigations have focused on CO_2 emission from volcanic settings [*Cardigos et al.*, 2005; *Caudron et al.*, 2012], this is the first to utilize midwater multibeam sonar data to study CO_2 gas release from an erupting submarine volcano.

In March 2010, we used a Kongsberg EM122 multibeam sonar system on *R/V Kilo Moana* (cruise KM1005) to image CO_2 bubble plumes in the water column above the summit of NW Rota-1 (Figure 1), an actively erupting seamount in the Mariana volcanic arc [*Embley et al.*, 2006; *Chadwick et al.*, 2008]. The main goal of this study was to determine how the bubble plumes related to the volcanic activity on the seafloor. Specifically, how they varied with time and how effective sonar data were at quantifying that variability, how and whether the plume geometry changed due to ocean currents, and how much the bubble plumes reflected

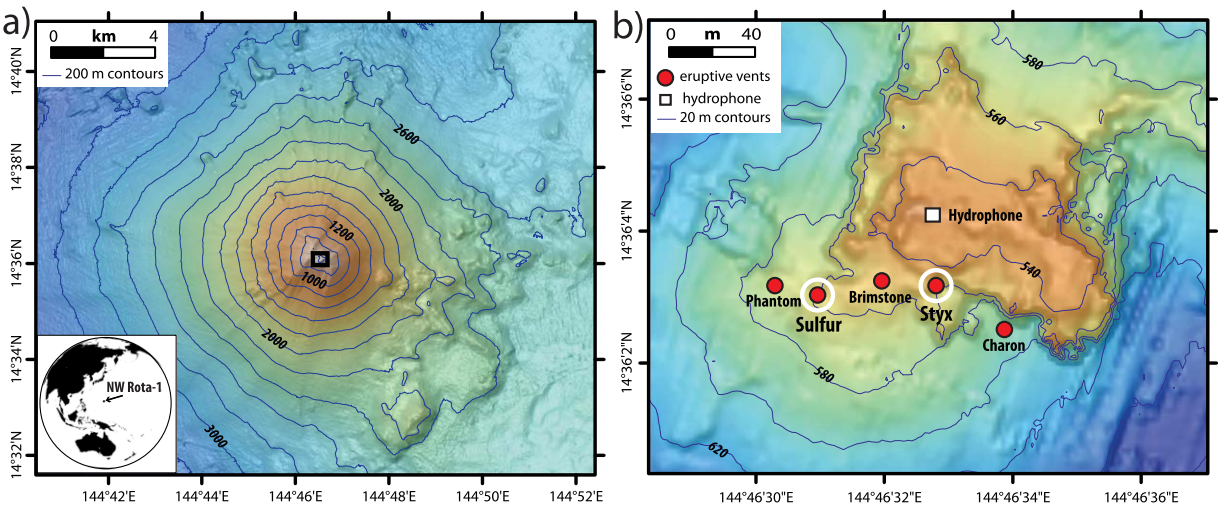

Figure 1. Maps of NW Rota-1 seamount. (a) EM300 multibeam bathymetry of NW Rota-1 (inset shows regional location). (b) High-resolution SM2000 multibeam sonar bathymetry of the summit of NW Rota-1 collected by ROV *Jason* in 2010, showing locations of five eruptive vents (red circles) and deployment site of portable hydrophone (white square). Only two of the five eruptive vents, Sulfur and Styx (white circles), were active during the multibeam 3-D-pass time series.

the intensity of eruptive output of the volcano. Analysis of these data could help determine how useful midwater multibeam data are at characterizing the bubble plumes at NW Rota-1 and how much they reveal about the underlying volcanic processes.

2. Background and Setting

NW Rota-1 is noteworthy as the first site where submarine eruptive activity was directly observed in 2004 [*Embley et al*., 2006]. Since then, it has remained in an apparently nearly continuous but variable state of activity through at least 2010. The eruption style is generally Strombolian—that is, primarily driven by magmatic degassing with a low mass-eruption rate and cyclic ejection of tephra or the slow extrusion of blocky lava [*Chadwick et al*., 2008; *Deardorff et al*., 2011; *Dziak et al*., 2012]. Degassing of CO_2 bubbles accompanies this Strombolian activity (Movie 1). The composition of the bubbles emitted at NW Rota-1 is 90% CO_2 and 10% H_2 [*Lupton et al*., 2008], and the chemistry of the hydrothermal plumes and vent fluids has been previously described [*Resing et al*., 2007; *Baker et al*., 2008; *Walker et al*., 2008; *Butterfield et al*., 2011].

The volcano's summit is at a depth of 517 m, and the eruptive activity is located at ~560 m on the steep south flank. Between 2003 and 2009, volcaniclastic debris accumulated downslope from a single eruptive vent named Brimstone. Then in August 2009, a major landslide removed that accumulated debris and transported it downslope to the southern base of the cone [*Chadwick et al*., 2012]. Dives with the *Jason* remotely operated vehicle (ROV) after the landslide in March 2010 found five eruptive vents evenly spaced along an east-west line spanning ~110 m, including the preexisting Brimstone vent (Figure 1). The eruptive activity at the individual vents was intermittent, cycling on-and-off from hour-to-hour and day-to-day. When active, the vents were either characterized by continuous passive degassing or by cyclic stronger explosive bursts, separated by pauses every few minutes. ROV video shows that CO_2 bubbles were emitted from the eruptive vents at a low level during passive degassing and in much larger quantities during the explosive bursts (Figure 2 and Movies 2 and 3). Gas bubbles were not emitted when the vents were inactive.

3. Field Methods and Terminology

3.1. Data Collection

During our 2010 fieldwork at NW Rota-1, we collected midwater data with the EM122 multibeam sonar (at an average ping rate of one every 4–6 s), both between and during *Jason* dives, and we experimented with various ways of surveying the bubble plumes over the summit, partly based on fortuitous sonar tests at the site the previous year [*Hughes-Clarke*, 2009]. Between *Jason* dives, we made repeated slow passes with the ship (at 0.5–5 knots) over the eruptive vents in order to image the bubble plumes in three dimensions ("3-D-passes," hereafter). Each ping of the sonar sends out sound in a 2-D "beam-fan" that is oriented perpendicular to the ship heading (Figure 3), recording a roughly 2-D slice through the 3-D object of interest (the

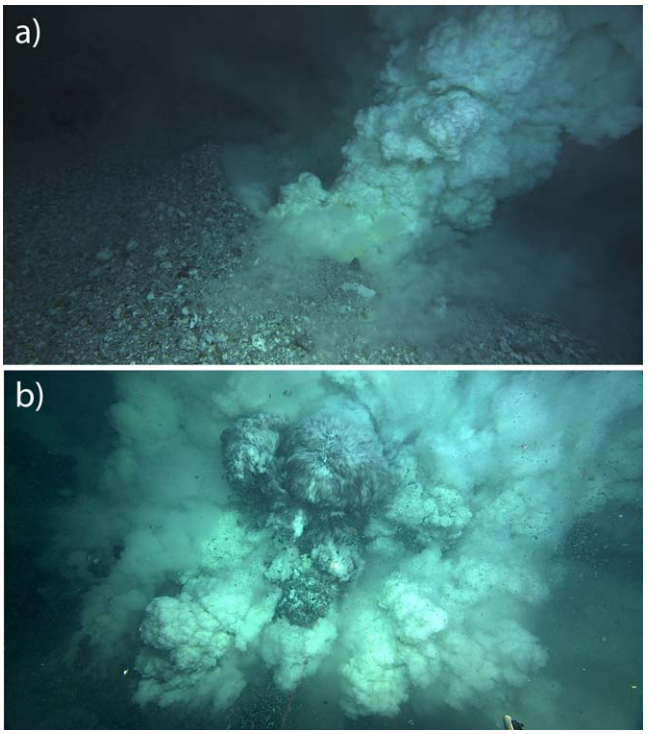

Figure 2. Video frame grabs from ROV *Jason*. (a) Sulfur eruptive vent (J2-495, 23:11:18, 28 March 2010, vent is 1.5 m across), characterized by continuous, quiet, passive degassing. (b) Styx eruptive vent (J2-494, 04:28:56, 27 March 2010, image is 3.5 m across), characterized by intermittent, loud, strong explosive bursts. Both vents were emitting CO_2 bubbles detected by the multibeam sonar, but only the explosive activity at Styx vent was detected by the hydrophone.

bubble plume). For resolving the plumes in 3-D, we found that the best results were obtained when the ship's forward speed was as slow as possible ($\leq$1 knot) so that it could collect as many 2-D slices though the bubble plume as possible. Effectively, each slow pass with the ship over the volcano summit ($\sim$30 min each) created a snapshot of the size, shape, and volume of the bubble plume during that time interval. Ship pitch and roll were recorded in real time and corrected for during routine multibeam data processing, which includes corrections for depth-dependent sound speed and refraction.

We also collected midwater data during some *Jason* dives when the ship was nearly stationary over various sampling sites on the seafloor, with a more-or-less constant heading. If the ship was located directly over an eruptive vent with its heading into the current, then these data recorded a time series of bubble clouds rising through the stationary vertical plane of the 2-D beam-fan, before they drifted down current. Consequently, these "2-D beam-fan" time series do not resolve the bubble plume in three dimensions, but instead provide a view of temporal variability and a measure of the rise rate of bubble clouds expelled during individual explosive bursts.

3.2. Data Processing

After the multibeam midwater data were collected, we analyzed the sonar files with FMMidwater, a QPS Fledermaus software module. Using this software, there are three ways of analyzing and displaying the midwater data: (1) as a series of 2-D beam-fans (each fan from a single sonar ping, Figure 3a), (2) as a 2-D "stacked-curtain" along the ship track, which summarizes the information from the beam-fans during each 3-D-pass (Figure 3b), or (3) as a 3-D "volume-object," which is a rendering of the volume with acoustic backscatter values above a chosen threshold for each 3-D-pass (creating a 3-D visualization of the bubble plume itself, Figure 3c). The stacked-curtains are like a deck of playing cards, viewed from the side, with each card representing a 2-D beam-fan, and the deck representing the entire swath. The stacked-curtain view collapses all of the 2-D beam-fans in a swath to 1-D at nadir, and displays the maximum signal level for every discrete range increment in each ping. The result is a 2-D vertical plane of strongest recorded sonar return, whose top edge follows the ship surface track. All the 3-D volume-objects presented here were created using the same minimum and maximum relative amplitude thresholds of -39 and $+5$ (in units of the raw amplitude values in the sonar file), to enable consistent comparison within the time series of 3-D passes. We chose a constant 3-D-volume pixel ("voxel") size of $1.5 \times 1.5 \times 1.5$ m for all the volume-objects. Movie 4 is a fly-through movie that helps visualize the relationship between the 2-D beam-fans, a 2-D stacked-curtain, and a 3-D volume-object for one 3-D-pass.

From these processing steps, we extracted the following quantifiable parameters for each 3-D-pass to track the character of the bubble plumes over time and to compare these sonar results with other independent

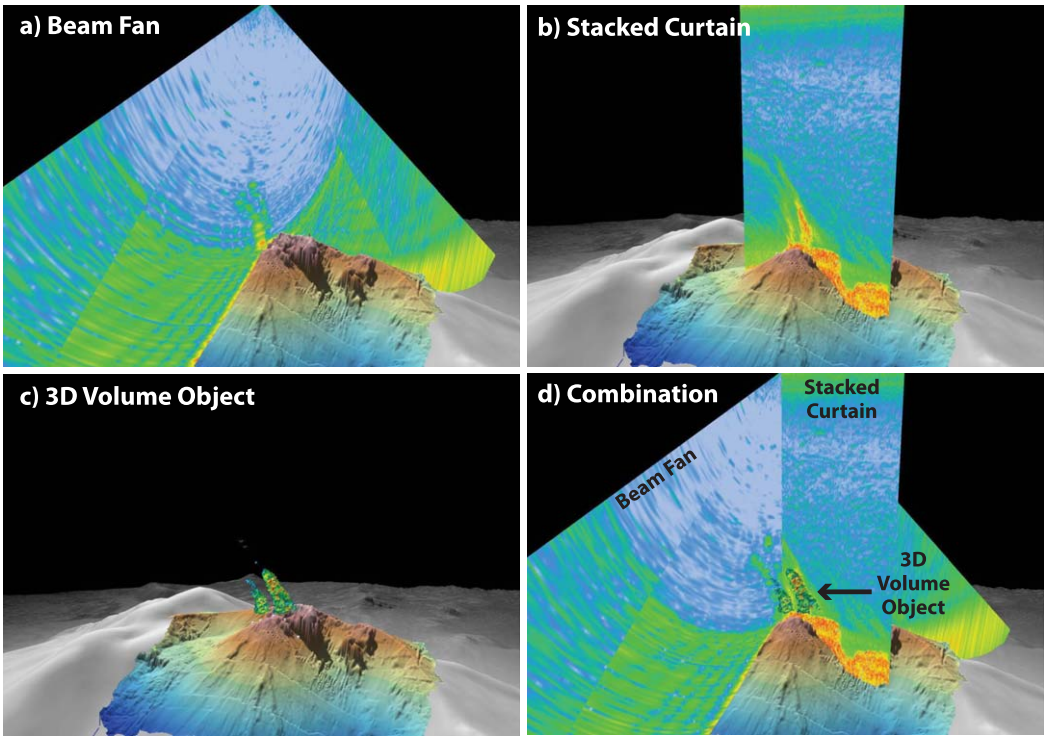

Figure 3. Oblique view showing relationship between three ways of visualizing the midwater multibeam sonar data: (a) 2-D beam-fan, the acoustic returns from one sonar ping, (b) 2-D stacked-curtain, a 2-D display along the ship track of maximum returns from the beam-fans collapsed to nadir, (c) 3-D volume-object, interpolated from threshold filtering of acoustic returns in the stacked-curtain, and (d) a combination of all three views. See also Movie 4.

datasets: (1) the depth of the top of the bubble plume, measured in the beam-fans, and (2) measured by the 3-D volume-objects (which are always deeper since the thresholds used to create them exclude some lower-amplitude data), (3) the highest amplitude of acoustic backscatter for each 3-D-pass, measured in the stacked-curtain, (4) the volume of the 3-D volume-object, and (5) the deflection direction and distance of the top of the 3-D volume-object, relative to the eruptive vent source. The calculated volume of the 3-D volume-objects is a relative acoustic measure of the extent of the bubble plume, but it is not the same as the actual volume of bubbles in the water column, which is unknown.

3.3. Data Comparisons

We compared the midwater multibeam sonar data to several other independent data sets collected on the same expedition, including ocean currents, underwater sound, and visual observations from the ROV. Time series data on the local ocean currents (velocity and direction versus depth) were obtained using *R/V Kilo Moana*'s hull-mounted Teledyne RDI 38 kHz acoustic doppler current profiler (ADCP). Current data were collected and processed using the University of Hawaii Data Acquisition System (UHDAS) [*Firing and Hummon*, 2010; *Firing et al*., 2012]. Data processing encompassed single-ping editing, vector averaging, and compass error estimation and correction. Sounds generated by NW Rota-1's eruptive activity were recorded with a "B-Probe" hydrophone (s/n 23) from Greeneridge Sciences, Inc. that was originally designed for marine mammal studies. The hydrophone was deployed on the seafloor at the volcano's summit (30 m from the nearest eruptive vent, Figure 1). The hydrophone is compact, self-contained (20 cm long), with a sensitivity of −152 dB relative to 1 V/μPa and a 16 bits data logger with a dynamic range of 96 dB (however, the system's internal noise limits this to a somewhat lower level). We chose a sampling rate of 1024 Hz, to focus on low-frequency sounds from the volcano. Our previous work at NW Rota-1 showed that acoustic amplitude recorded by hydrophones was a good measure of the intensity of explosive activity at the eruptive vents [*Chadwick et al*., 2008]. Visual observations at the eruptive vents during *Jason* dives also provided valuable information about the character of the eruptive activity in 2010, which vents were active and when, and basic information about the size range and ascent velocity of the CO_2 bubbles.

4. Results

In total, >95 h of midwater multibeam data were collected over a 12 day period, about half were aquired while conducting 120 separate 3-D-passes over the summit vents, and half while the ship was mostly stationary during *Jason* dives. Bubble plumes were observed in the midwater data during every 3-D-pass, showing that one or more eruptive vents were emitting CO_2 bubbles throughout the 2 week cruise, at least at a low flux. Here we concentrate on an optimal subset of the data: a continuous 19 h time series of 29 separate 3-D-passes over the vents, collected at $\leq$1 knot, between *Jason* dives J2–494 and J2-495 (section 4.2), and a 1.5 h time series of 2-D beam-fan data collected directly over Styx vent (Figure 1) during *Jason* dive J2-494 (section 4.5). Before presenting the multibeam data, we discuss ROV visual observations at the eruptive vents (section 4.1), and later compare the multibeam data to the ADCP (section 4.3), and hydrophone (section 4.4) data sets.

4.1. Seafloor Observations During Jason ROV Dives

ROV dive video provides important ground-truth information for interpreting and validating the bubble plume data, including the locations of the eruptive vents on the seafloor, observations of the style and temporal variability of the degassing at specific vents, and estimates of the size and ascent rate of CO_2 bubbles. Each of the eruptive vents at NW Rota-1 is only 1–2 m in diameter. Scale in Jason imagery is determined by camera-mounted lasers that are spaced 10 cm apart. During eruptive activity at NW Rota-1, H_2O, SO_2, and CO_2 are degassed from the magma, but they each behave differently: H_2O vapor quickly condenses, SO_2 dissolves in seawater, and CO_2 remains a gas [*Chadwick et al*., 2008]. The SO_2 reacts rapidly with seawater, forming sulfuric acid and tiny sulfur droplets in a billowing, yellowish cloud [*de Ronde et al*., 2005; *Resing et al*., 2007; *Butterfield et al*., 2011]. In contrast, the CO_2 escapes as streams of clear bubbles that immediately separate from the sulfur-rich plume because they have greater buoyancy [*Lupton et al*., 2008]. Thus, the behavior of the CO_2 and SO_2 are easy to distinguish visually. Video analysis shows that CO_2 bubbles emitted from the vents ranged in diameter between 0.5 and 3.0 cm, with most between 1 and 2 cm. It is likely that even larger bubbles are emitted during the most vigorous explosive activity when visibility is poor. The ascent rate of the bubbles was measured to be $\sim$30 cm/s at the seafloor in ROV video. Using this value and the depth of the vents (560 m), a crude estimate for the lifetime of the bubbles if they rose at this constant rate all the way to the ocean surface is 31 min. However, the actual rise time will be different since the bubbles will dissolve, get smaller, and perhaps fragment, processes that could either speed up or slow their ascent rate as they rise.

During the two *Jason* dives before and after the 19 h time series of 3-D-passes (J2-494 and J2-494), only two of the five eruptive vents were observed to be active and emitting CO_2 bubbles and they each had distinctly different activity. Sulfur vent (Figures 1 and 2a) was seen to be passively and continuously degassing CO_2 bubbles (Movie 2). In contrast, Styx vent (Figures 1 and 2b) had intermittent violent explosive bursts that expelled CO_2 bubbles in larger quantities (Movie 3), but in between the bursts no bubbles were emitted. Bubble size appeared to be related to the intensity of the eruptive bursts with the largest bubbles being produced by the largest explosive bursts at Styx vent. Another important difference between these contrasting styles of activity is that the passive degassing at Sulfur was relatively quiet acoustically, whereas the explosive bursts at Styx vent produced sound that was recorded by the in situ hydrophone (determined by comparing simultaneous ROV vent observations and acoustic data). Therefore, the hydrophone data provide a quantitative time series record of the explosive degassing at Styx vent (discussed below in section 4.5). That record shows that the average explosive burst duration was 3.6 $\pm$ 2.5 min separated by pauses of about the same length (2.9 $\pm$ 2.9 min), but the amplitude and frequency of the activity varied significantly with time. Over longer time periods, Styx cycled between several hours of eruptive activity, followed by several hours of inactivity.

4.2. Multibeam 3-D-Pass Time Series

The 19 h time series of 29 3-D-passes extended from 14:15 on 27 March to 09:37 on 28 March (all times UTC, 10 h behind local time). Most of the 3-D-passes were collected along a 600 m long line oriented WNW-ESE (Figure 4), except during five passes (15–19) oriented orthogonally (SSW-NNE) midway through the time series (00:33–02:32 on 28 March). From one pass to the next, the ship drove in the opposite direction along the line. To analyze and compare each 3-D-pass, we created a 2-D stacked-curtain (maximum acoustic amplitude in the beam-fans displayed along the ship track) and a 3-D volume-object (volume of highest

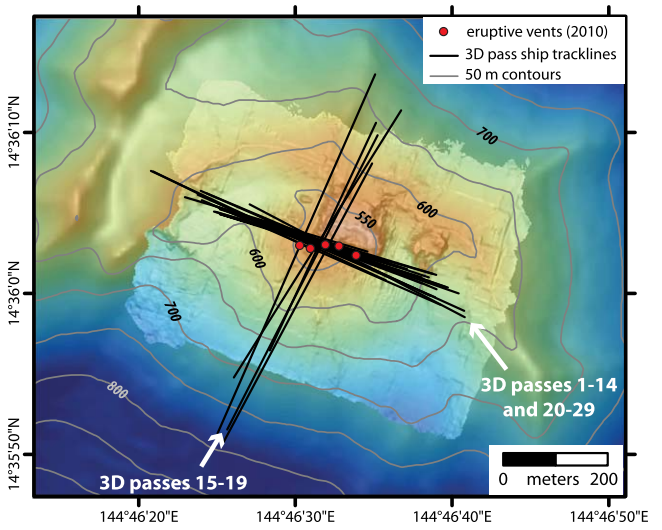

Figure 4. Map showing location of 29 "3-D-passes" made over the summit of NW Rota-1 at ≤1 knot while collecting midwater multibeam data during a 19 h time series to image the bubble plumes in three dimensions. The orientation of the passes was changed temporarily during 3-D-passes 15–19. ROV-based high-resolution bathymetry (2 m grid) is overlain on lower-resolution ship-based bathymetry (20 m grid).

acoustic returns using constant amplitude thresholds and voxel size). Figure 5 shows a subset of six of the stacked-curtain views, and Movie 5 presents a time-lapse movie of all 29 stacked-curtains. Similarly, Figure 6 shows a subset of the volume-objects and Movie 6 displays a time-lapse movie of them from all the 3-D-passes. The change in orientation of the survey lines midway through the time series is reflected in the stacked-curtain views (since they are best viewed perpendicular to the ship track), but not the volume-objects (since they can be viewed from any angle).

Bubble plumes are observed in every pass (Figure 5 and Movie 5), and in most there are two distinct plumes that originate on the seafloor from Sulfur and Styx vents, which are located 55 m apart at 560 m depth. The bubble plumes generally extended up to depths between 350 and 250 m before dissipating, and sometimes as high as 150 m depth (rise heights of 200–400 m), but never all the way to the ocean surface. In the time series, the plume from Sulfur vent is generally more continuous vertically, whereas the plume from Styx vent is more discontinuous with distinct "puffs," reflecting the difference in the style of degassing at the two vents.

In the stacked-curtain views, the (nonplume) acoustic returns in the background are affected by three noticeable phenomena. First, there is a persistent zone of elevated backscatter near the bottom (below the white dashed lines in Figure 5), which is caused by sidelobe echoes from the adjacent seafloor. Second, many plankton and fish have swim bladders filled with air which reflect sound that creates a "deep scattering layer" [*Medwin and Clay*, 1998]. These organisms migrate vertically diurnally, coming up toward the surface at night and moving deeper during the day. This diurnal vertical migration is evident in the 19 h stacked-curtain time series (Figure 5 and Movie 5), which started at night, continued through sunrise (at 20:20 UTC, during 3-D-pass 10), and ended an hour after sunset (at 08:32 UTC, just before 3-D-pass 28). The background color in the stacked-curtain time series turns from green to blue (from higher to lower backscatter), coincident with the change from night to day. Thus, the signal-to-noise ratio in the midwater multibeam data is better during the 3-D-passes collected during daylight hours. The third phenomena visible in the background of the stacked-curtain views are artifacts of unknown source that we speculate are due to interference with some other sound source from the ship. These artifacts appear similar to the real bubble plumes, in that they originate at the seafloor and extend up into the water column at an angle (short arrows in Figure 5), but they are inconsistent in location from pass to pass, and are weaker in amplitude than the real plumes. It is clear they are artifacts because they are consistently inclined in the direction of ship motion and change orientation on every subsequent pass (Movie 5), unlike the real bubble plumes which move in concert with the ocean currents (see section 4.4, below).

In the 3-D volume-object views (Figure 6 and Movie 6), the bubble plumes are more limited in vertical and lateral extent than in the stacked-curtains, because the 3-D volume-objects are derived from a subset of the acoustic returns above a minimum threshold. Nevertheless, two distinct plumes from Sulfur and Styx vents are visible on many of the passes. In addition, there are two obvious changes that occur during the 19 h time series. First, the 3-D volume-objects become noticeably smaller and less distinct during passes 15–19 (Figure 6 and Movie 6). Second, most of the 3-D volume-objects are nearly vertical at their bases and bend toward the west in their upper halves, except for a period midway through the time series when they extend to the east during passes 12–14, then their orientation is unclear during the minimal plumes in

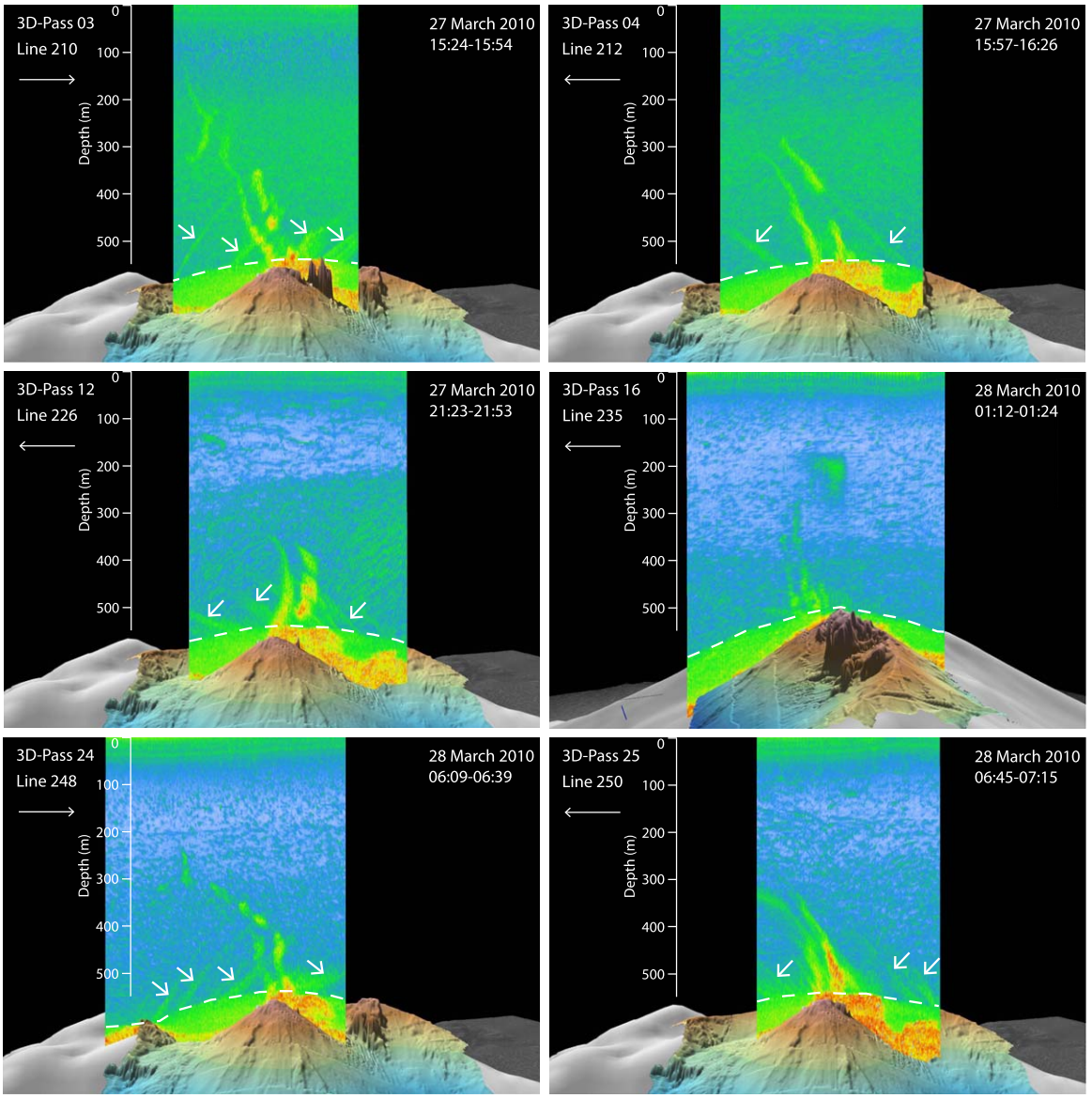

Figure 5. Subset of 2-D stacked-curtain views of bubble plumes above NW Rota-1 during the 3-D-pass time series. Colors indicate relative amplitude of acoustic returns (blue = low, red = high). The 3-D-pass number, line number (file ID), ship travel direction (arrow in upper left), and date/time are indicated. Two distinct bubble plumes are visible in most views (from Sulfur and Styx vents) but they vary with time (see text). Deep scattering layer is evident in Figures 5a and 5b as light green in background (higher acoustic return) for 3-D-passes collected during local nighttime, but is absent in Figures 5c–5f during local daylight (light blue background; lower acoustic return). Small white arrows point to acoustic artifacts that are inclined in the direction of ship travel. Data below dashed white lines include sidelobe echoes from the seafloor. See Movie 5 for all the stacked-curtain views in the 3-D-pass time series.

passes 15–19, and they resume their more robust size and westward inclination thereafter (Figure 6 and Movie 6).

One qualification to these observations is that the N-S lines (passes 15–19) effectively imaged the bubble plumes in lower resolution than the E-W lines for the following reasons: (1) the N-S lines were oriented perpendicular to the axis of the bubble plumes and therefore imaged the plumes with fewer sonar pings, and (2) the N-S lines had to be driven at a faster speed (1–2 knots) because of current and wind directions, also contributing to fewer sonar pings through the bubble plumes. However, we believe our 3-D-pass comparisons are still valid, because the stacked-curtain views for passes 15–19 suggest that weaker plumes were still discernable in the midwater data, consistent with the lack of robust plumes in the 3-D volume-objects. In other words, bubble plumes were still discernable in the midwater data during passes 15–19 but they were distinctly lower in amplitude, which is also consistent with the hydrophone observations (section 4.4, below).

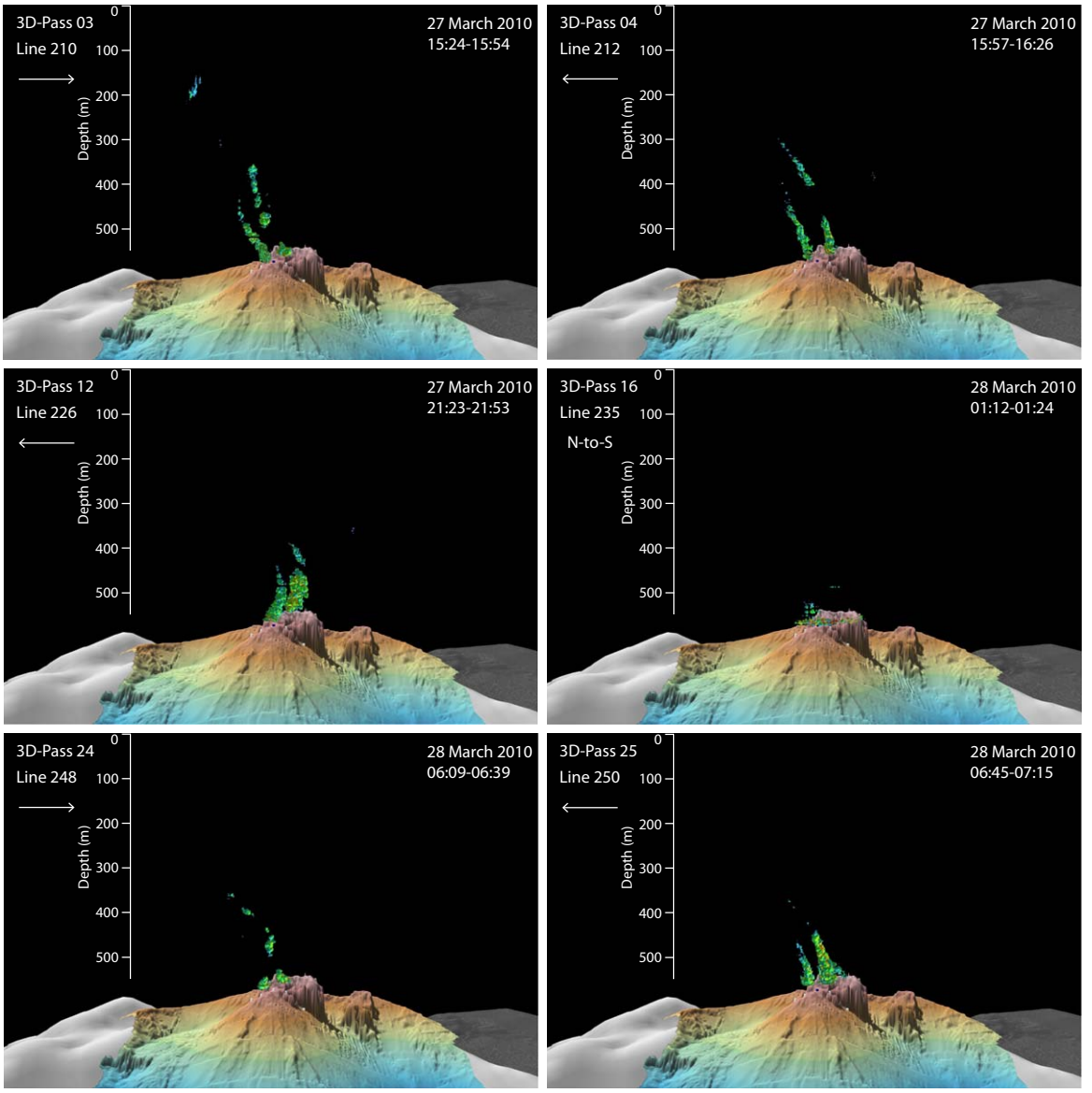

Figure 6. Subset of 3-D volume-object views of bubble plumes above NW Rota-1 during the 3-D-pass time series. The 3-D-pass number, line number (file ID), ship travel direction (arrow in upper left), and date/time are indicated. Two distinct bubble plumes are visible in most views (from Sulfur and Styx vents) but they vary with time (see text). See Movie 6 for all the volume-object views in the 3-D-pass time series.

4.3. Comparison With ADCP Data of Ocean Currents

Data from the ADCP on *R/V Kilo Moana* provide information on the ocean currents at NW Rota-1 during the multibeam surveys. The ADCP data give current velocity and direction versus depth (binned in 24 m depth increments). For this analysis, we plot the ADCP data averaged over the time intervals when the ship was passing over the vents during each 3-D-pass. Figure 7 shows a subset of these plots that correspond to the same 3-D-passes in Figures 5 and 6. Movie 7 is a time-lapse movie with each frame showing the currents averaged during each 3-D-pass. Movie 8 is a more continuous view of the currents during the 3-D-pass time series, with a smaller 5 min time window for each frame.

The ADCP data show that the largest current velocities (20–40 cm/s) are near the surface ($<$300 m) and are generally toward the west (Figure 7), and are most likely influenced by prevailing winds. The deeper currents ($>$300 m) have smaller velocities (10–20 cm/s), are more variable in their direction (Figure 7), and are more clearly influenced by the tidal cycle. For example, the deepest currents are directed westward on passes 1–11 (a 7 h span), then switch to the east during passes 12–19 (5 h), and back to the west for the

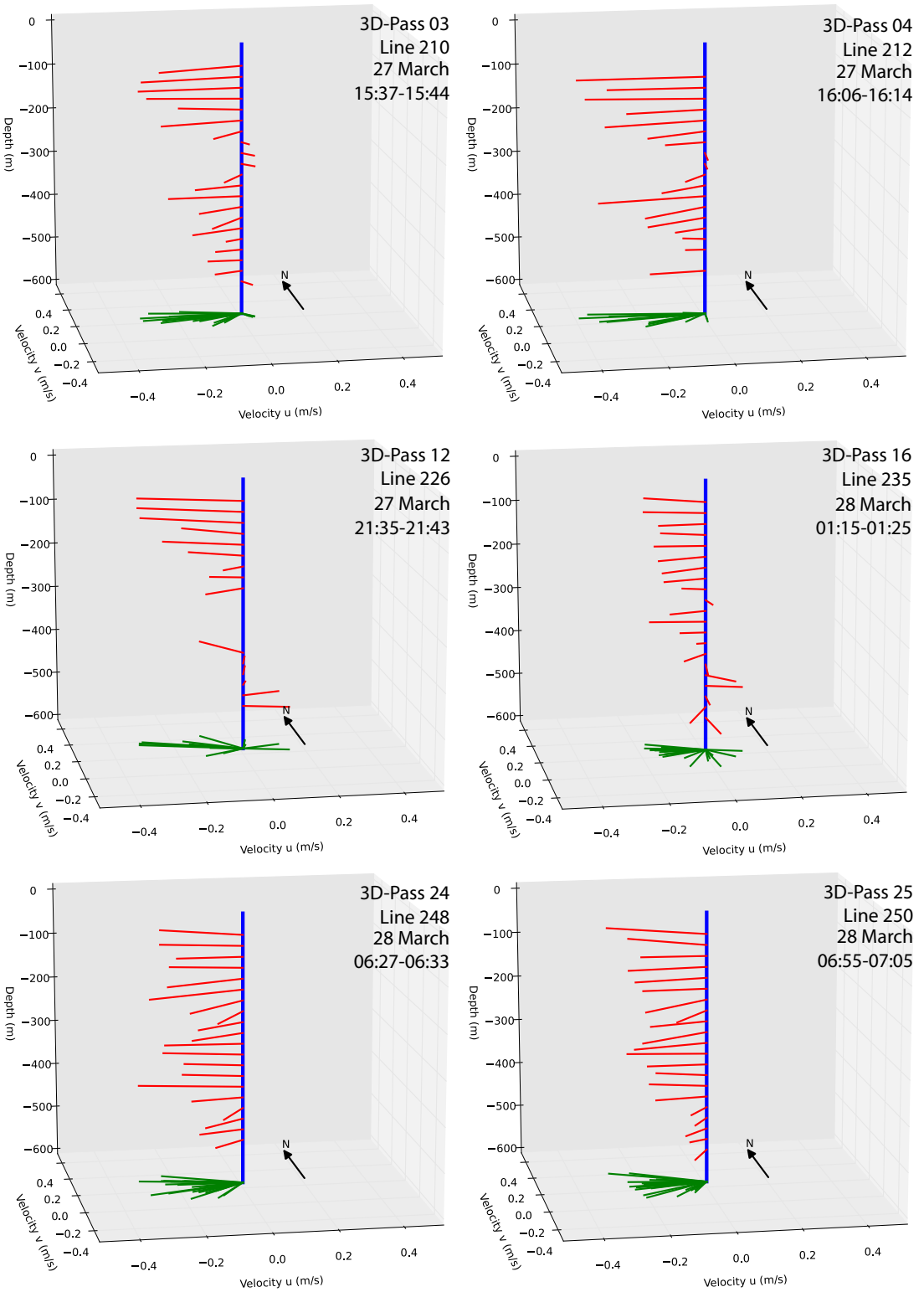

Figure 7. Subset of ADCP data collected during the 3-D-pass time series, averaged when the ship was directly over the eruptive vents during the individual passes. Vertical blue line represents approximate location of NW Rota-1 summit, red bars show velocity and direction of ocean current binned at 24 m depth intervals, green bars show projection of red bars onto the bottom of plots to aid in visualizing their directions. The 3-D-pass number, line number (file ID), and date/time are indicated on each plot. Note that shallower currents generally have higher velocities, and their direction is predominantly westward except in Figures 7c and 7d when the deepest currents temporarily turned eastward. See Movies 7 and 8 for a time-lapse view of similar plots during the entire 3-D-pass time series.

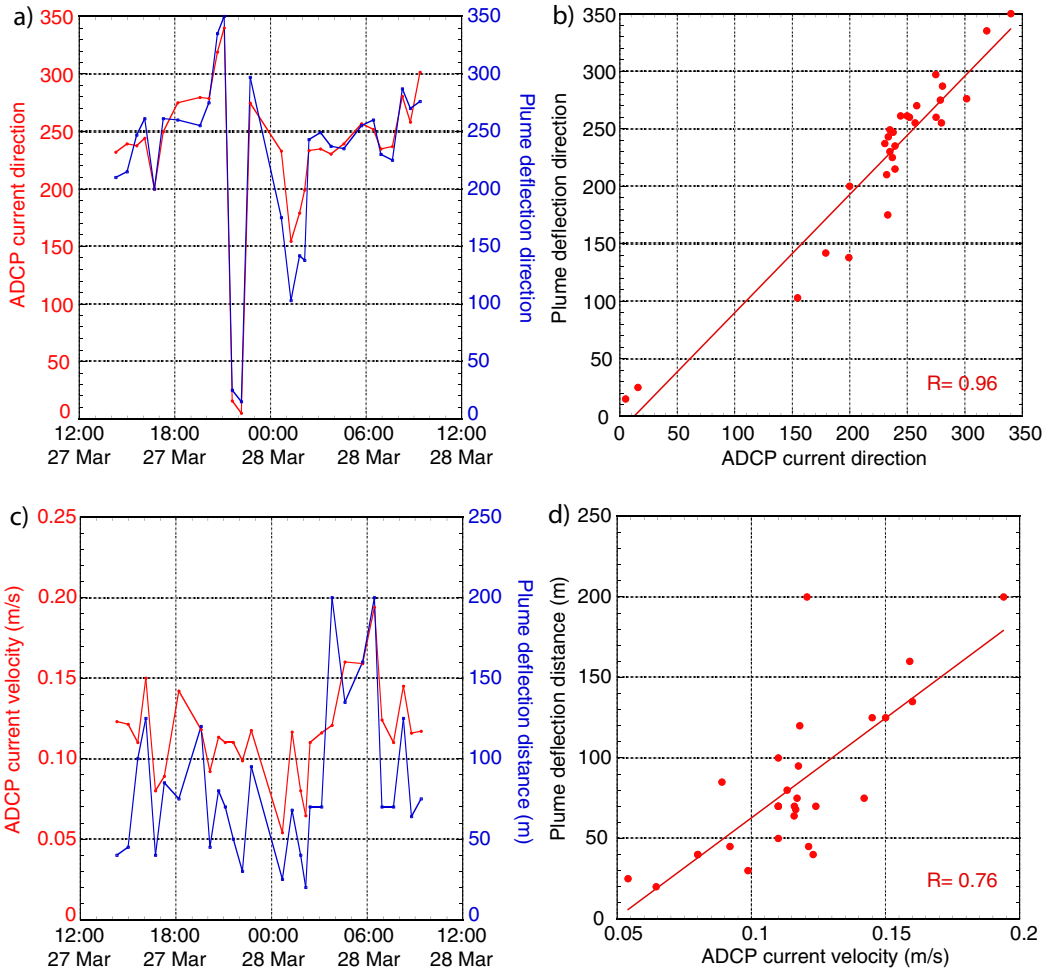

Figure 8. Plots showing comparison of ADCP data and bubble plume orientation during 3-D-pass time series. (a) ADCP current direction and bubble plume deflection direction for each 3-D-pass versus time. (b) Correlation of plume deflection direction versus current direction. (c) ADCP current velocity and bubble plume deflection distance for each 3-D-pass versus time. (d) Correlation of plume deflection distance versus current velocity. ADCP data are averaged when ship was over the vents and over the depth interval of plume bending. Plume deflection direction and distance are measured from the eruptive vent to the top of the plume in the 3-D volume-object for each 3-D-pass. Red lines in Figures 8b and 8d are linear least squares fits to the data; R values are correlation coefficients.

rest of the time series (Movie 7). This coincides with the same passes when the plumes in the 2-D stacked-curtains (Figure 5) and 3-D volume-objects (Figure 6) are bent to the east rather than to the west.

To better illustrate this correspondence, the deflection direction and distance of the 3-D volume-objects (measured from the eruptive vent to the top of the deflected plume) were plotted versus the ADCP current direction and velocity (averaged over the depth interval of the deflected plume) in Figure 8. For direction of currents and plume deflection, the correlation is excellent; for deflection distance and current strength, the correlation is very good. This confirms that the multibeam midwater data accurately resolve the three-dimensional shape of the bubble plumes in a changing ocean current field. The stronger currents in the upper water column also explain why the bubble plumes often are bent in a dog-leg fashion, nearly vertical near the seafloor and inclined above a depth of 300–400 m.

4.4. Comparison With Hydrophone Data Characterizing Eruptive Activity

The portable hydrophone we deployed at NW Rota-1 was similar to one used by *Chadwick et al.* [2008], who showed that the recorded acoustic amplitude was a good quantitative measure of eruptive intensity. As before, the hydrophone was deployed on the seafloor at the volcano summit (Figure 1; 30 m north and 40 m shallower than Styx vent). A convenient way to display the temporal variability of the hydrophone data is to plot the root-mean square (RMS) of the acoustic amplitude in digital units, averaged every second.

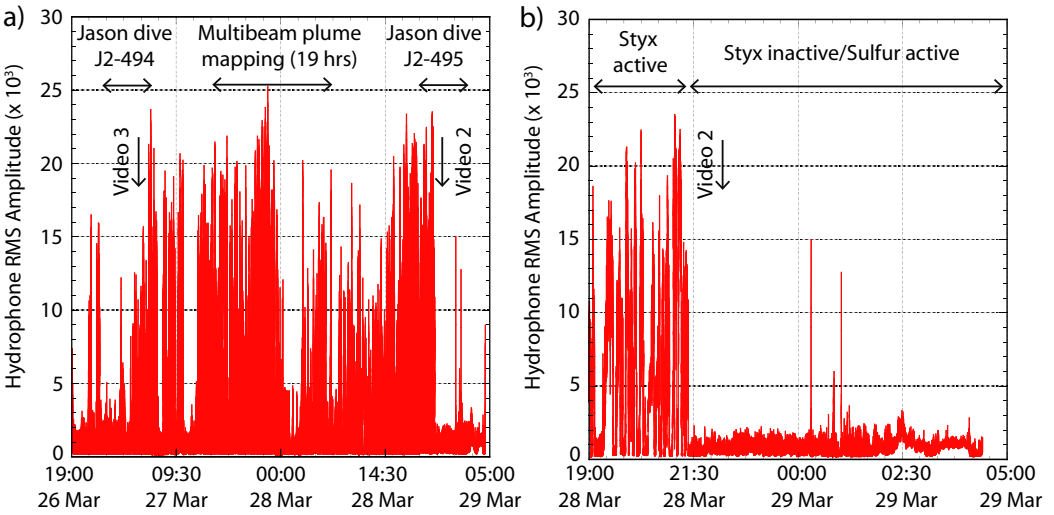

Figure 9. (a) Plot of portable hydrophone data recorded while deployed on seafloor at the summit of NW Rota-1 (see Figure 1), for a period of 2.5 days, including *Jason* dive J2-494, the 19 h 3-D-pass time series, and dive J2-495. Hydrophone RMS amplitude (in digital units, averaged every second) reflects the intensity of the eruptive activity at Styx vent (30 m away), which varied significantly during this time period. (b) Hydrophone record during Jason dive J2-495, showing times when Styx vent was active and inactive. Vertical arrows show times of visual observations at Sulfur and Styx vents in Movies 2 and 3.

Figure 9a shows a plot of RMS amplitude from the portable hydrophone during the 19 h multibeam time series and the *Jason* dives immediately before and after (J2-494 and J2-495). The ROV visited all the eruptive vents during both dives, and these visual observations confirm that only Sulfur and Styx vents were degassing CO_2, and only Styx was experiencing explosive bursts (Figure 2). They also confirm that the highest hydrophone amplitudes were recorded when Styx was the most active, and when the activity at Styx shut off that the acoustic amplitudes dropped to low levels, even when Sulfur vent remained active (but only passively degassing). For example, Styx vent shut off abruptly midway through dive J2–495 coincident with a drop off of hydrophone RMS amplitude (Figure 9b), despite Sulfur vent remaining active through the rest of the dive.

We compared the hydrophone data to the 19 h multibeam time series to determine if the changes observed in the bubble plumes reflect variations in explosive degassing activity at the eruptive vents, in this case, at Styx vent. We compared the following measures from the multibeam results to the hydrophone data: the height and calculated volume of the 3-D volume-objects, and the maximum acoustic amplitude measured in the 2-D stacked-curtains for each of the 29 3-D-passes. To do so, we had to take into account that a burst of bubbles from the vent requires a finite amount of time to rise from the vent to the plume top where they would be imaged by the multibeam; during each pass the bubbles already at the top of the plume would have been expelled from the vent (and created sound recorded by the hydrophone) tens of minutes beforehand. Comparisons of mutibeam data to the maximum hydrophone RMS amplitude recorded during the previous 30 or 60 min yielded similar results, but using an hour gave slightly better correlations, so that value was adopted in our comparison of the two data sets. Figure 10 shows plots of the hydrophone RMS amplitude during the hour preceding the same subset of 3-D-passes shown in Figures 5–7. Movie 9 is a time-lapse movie of similar plots for all the 3-D-passes that can be compared to Movies 5, 6, and 7. Movie 10 combines the four 3-D-pass time series (from stacked-curtain, volume-object, ADCP, and hydrophone) in the same frame so they can be more easily compared.

Fortunately, there was a significant change in eruptive output at Styx vent during the 19 h 3-D-pass time series, providing a good test of how well the multibeam and hydrophone data covaried, and we found a strong correlation between the two. To more clearly illustrate this, we compared the hydrophone and multibeam time series (Figure 11). The correlations between the multibeam bubble plume parameters and the acoustic measures of eruptive intensity show that the size and volume of the bubble plumes reflected the strength of the volcanic activity occurring on the seafloor, although unsurprisingly there is some scatter given the complexity between total acoustic energy and the bubble flux. In other words, the midwater multibeam data captured the temporal variability of the bubble plumes that are a meaningful manifestation of

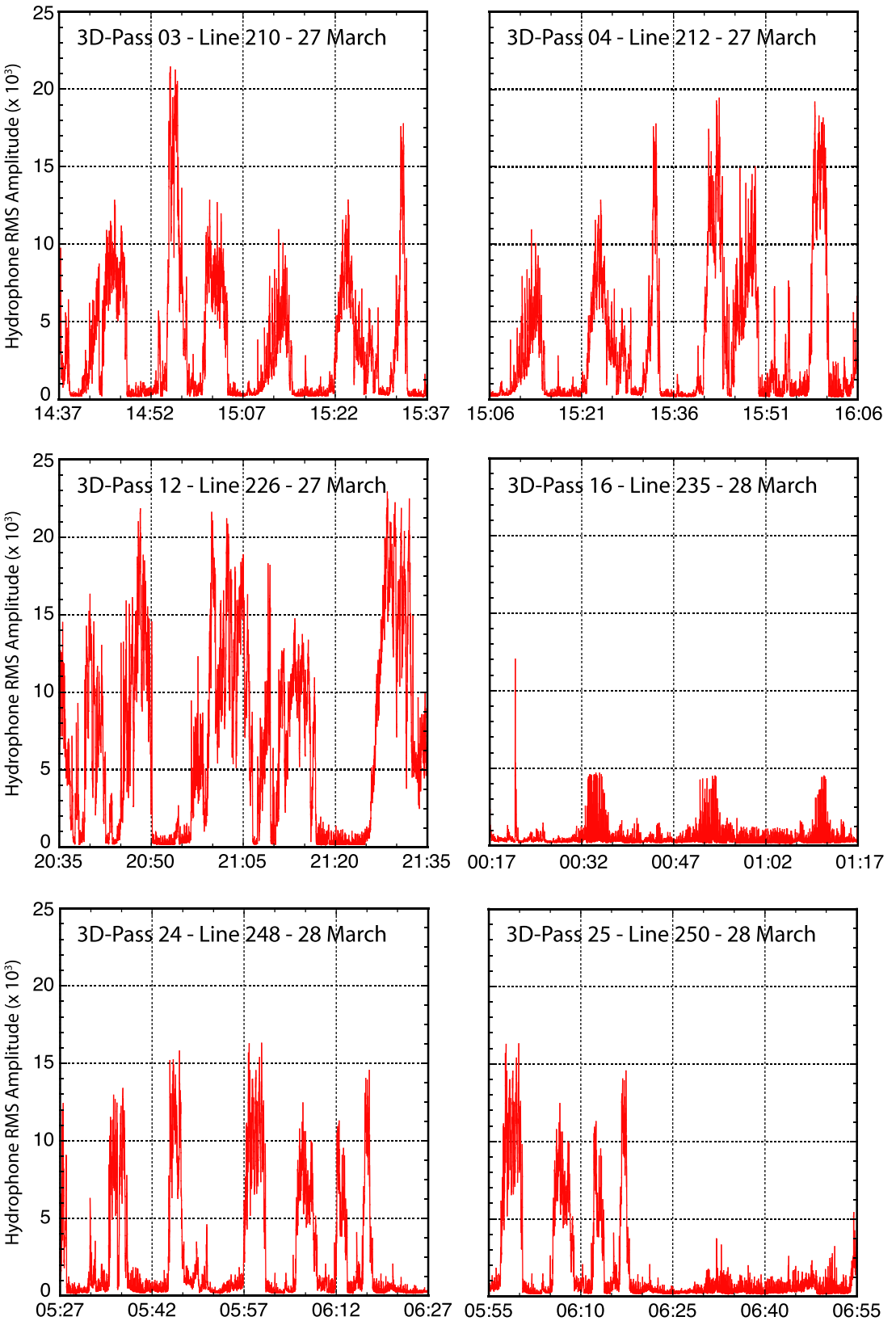

Figure 10. Subset of hydrophone data collected during the 3-D-pass time series, presented as plots of RMS amplitude (in digital units, averaged every second) during the hour preceding the time when the ship was first over the eruptive vents. The RMS amplitude is directly related to the vigor of eruptive activity at Styx vent, characterized by explosive bursts every few minutes. Note high levels in passes 1–14, low levels in 15–19, and moderate level in 20–29. See Movie 9 for a time-lapse view of similar plots during the entire 3-D-pass time series.

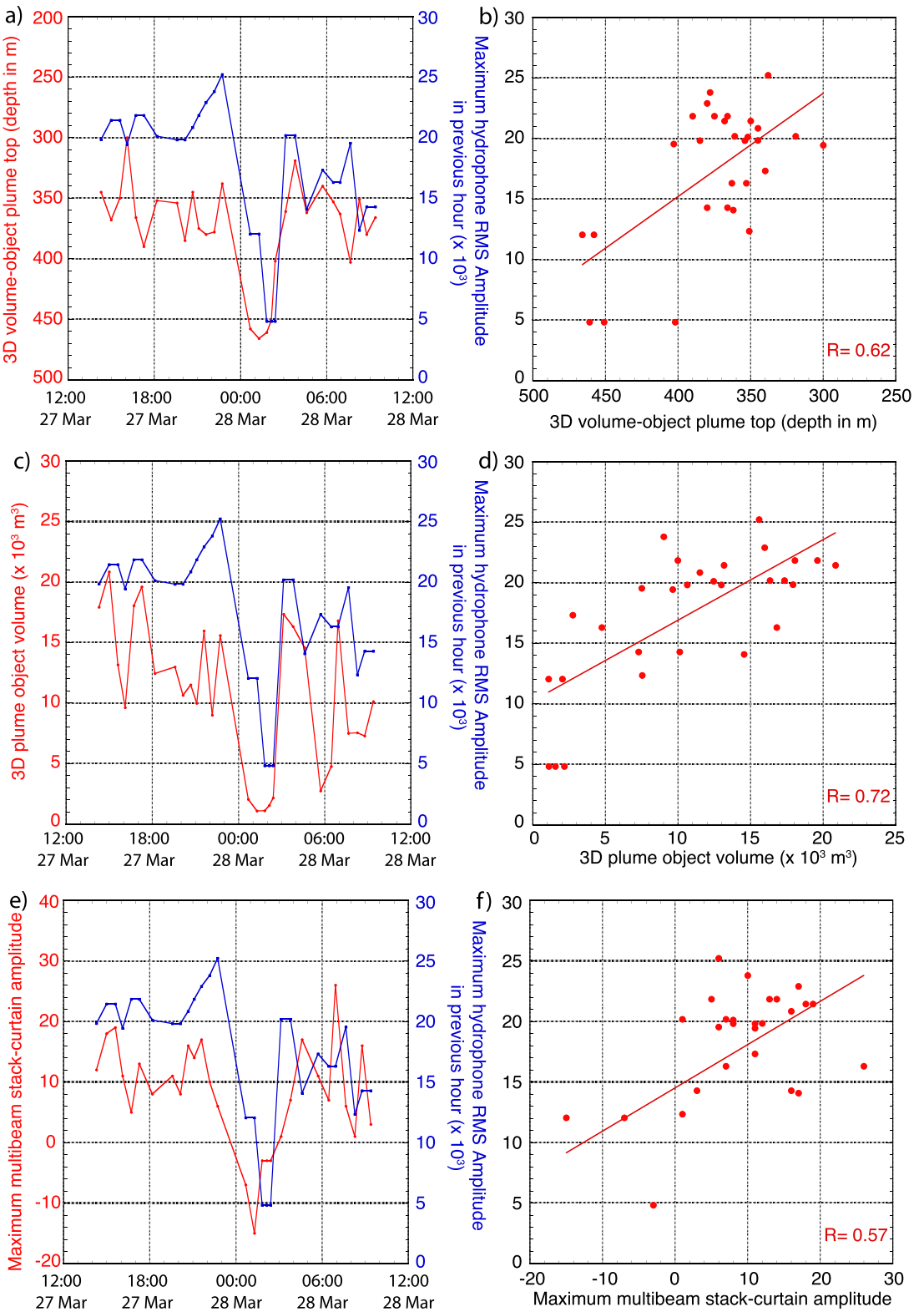

Figure 11. Plots showing comparisons of portable hydrophone data and bubble plume parameters during 3-D-pass time series. (a) Depth of top of 3-D volume-object (red) and hydrophone RMS amplitude (blue) for each 3-D-pass versus time. (b) Correlation of 3-D plume top and hydrophone amplitude. (c) Calculated volume of 3-D volume-object (red) and hydrophone RMS amplitude (blue) for each 3-D-pass versus time. (d) Correlation of 3-D object volume and hydrophone amplitude. (e) Maximum amplitude in bubble plume stacked-curtain (red) and hydrophone RMS amplitude (blue) for each 3-D-pass versus time. (f) Correlation of stacked-curtain amplitude with hydrophone amplitude. Red lines in Figures 11b, 11d, and 11f are linear least squares fits to the data; R values are correlation coefficients.

dynamic volcanic processes at the source. Similar results are obtained if we quantify the hydrophone data as the percentage of time the vent was active (instead of maximum RMS amplitude) during the hour preceding the start of each 3-D-pass.

The correlation of the hydrophone data with the 3-D plumes shows that they were mostly produced by the activity at Styx, while the continuous degassing at Sulfur alone was insufficient to create a robust 3-D volume-object (with the thresholds we picked). The highest multibeam amplitudes were produced by the plumes from Styx vent, so 3-D plume height, 3-D plume volume, and maximum amplitude in the multibeam stacked-curtains all correlate well with hydrophone RMS amplitude (Figure 11). In contrast, the hydrophone amplitudes correlated poorly with the beam-fan or stacked-curtain plume heights, because they can be lower in amplitude and produced by the continuous, nonexplosive and quieter activity at Sulfur vent when Styx is inactive. This explains why lower-amplitude plumes were imaged in the beam-fans or stacked-curtains during every 3-D-pass, regardless of whether the hydrophone data showed that Styx was active or not. There always was passive degassing going on, but not always explosive degassing. We suspect that the latter produces larger bubbles (and greater acoustic amplitudes) than the former.

4.5. Multibeam 2-D Beam-Fan Time Series

Just before the 19 h 3-D-pass time series, during *Jason* dive J2-494, there was a 1.5 h period when the ROV was working on the seafloor at Sulfur and Phantom vents and the ship was nearly stationary over Styx vent with an easterly heading (02:55–04:25 on 27 March). This position and orientation was optimal (and rare) for visualizing clouds of bubbles being intermittently expelled from Styx vent and rising through the multibeam's 2-D beam-fan (oriented perpendicular to the ship's heading). The bubble clouds from individual explosive bursts appear somewhat like "puffs" or "smoke signals" (circular blobs of high acoustic reflectivity) rising from the seafloor in the beam-fan view to ~100 m above the vent (Figures 12a and 12b and Movie 11), until the westward ocean current carried them out of the plane of the beam-fan. During this time, the hydrophone data show that Styx vent was producing intermittent explosive bursts, later confirmed when the ROV visited the vent from 04:20–05:17. The RMS acoustic amplitude of the bursts was initially relatively low but gradually increased during the second half of the dive (Figure 9a).

From these 2-D beam-fan data, a rise rate of bubble clouds from Styx vent was determined to be 25–30 cm/s (Figures 12a and 12b), consistent with the ROV-based visual observations on the seafloor (section 4.1). Another way of visualizing this is in a stacked-curtain view of the same data (Figure 12c). In this case, with the ship stationary, the horizontal axis of the stacked-curtain represents time (rather than distance, as in the 3-D-passes), and the inclined areas of high acoustic amplitude show individual bubble clouds rising ~100 m from the seafloor over a span of ~5 min (Figure 12c). Overlaying the hydrophone time series on the stacked-curtain (black curve in Figure 12c) shows that an explosive burst preceded the rise of a bubble cloud by ~1 min (roughly the time it took for the bubble cloud to rise at ~30 cm/s from the eruptive vent at 560 m, above the shallowest seafloor in the 2-D stacked-curtain at 540 m, and become visible in the midwater multibeam data). These data show that the intermittent explosive bursts at Styx vent with durations of only a few minutes produce individual "puffs" or clouds of bubbles that are visible in the 2-D beam-fan multibeam data, and are also evident in the 3-D-passes.

5. Discussion and Conclusions

Collection of midwater data is now possible with modern multibeam sonar systems, but this option increases the amount of recorded data (and the time to process it) by about an order of magnitude compared with conventional seafloor mapping, so it comes with a cost and may not always be practical or desirable. One of the goals of this project was to determine if the collection of midwater multibeam data over an active degassing submarine volcano provided useful information. The answer is yes.

The most useful ways of collecting the midwater multibeam data to characterize the bubble plumes at NW Rota-1 were either: (1) to drive the ship very slowly ($\leq$1 knot) over the eruptive vents repeatedly to create a time series to characterize the plume in three dimensions over time ("3-D-passes"), or (2) to collect data when the ship was nearly stationary over the eruptive vents to document the rise of bubble clouds in two dimensions ("2-D beam-fans"). The 3-D-passes provide a synoptic view of the plume over minutes to hours, whereas the 2-D beam-fans show variations in plume behavior over seconds to minutes.

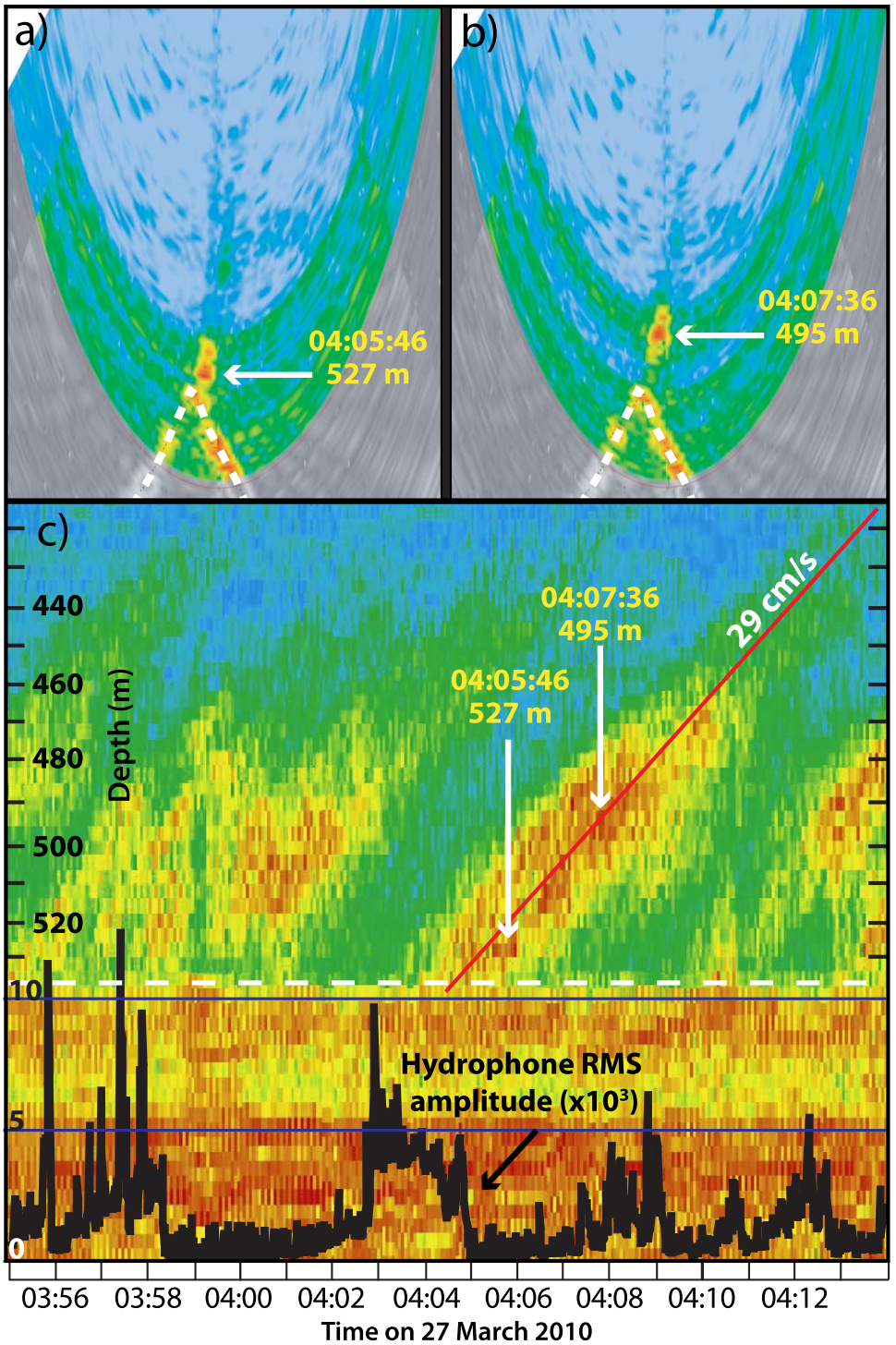

Figure 12. Multibeam midwater data from 03:55–04:14 on 27 March (file ID = line 200), collected while the ship was stationary over Styx vent. (a) The 2-D beam-fan at 04:05:46 showing circular bubble cloud centered at 527 m rising above the top of the seamount (white dashed line). (b) Similar 2-D beam-fan at 04:07:36 with the bubble cloud centered at 495 m, a rise of 32 m in 110 s, or a rise rate of 29 cm/s. (c) The 2-D stacked-curtain view of the same time period (vertical axis is depth, horizontal axis is time). Arrows point to times when the individual beam-fans in Figure 11a and 11b were collected. Solid red line shows a rise rate of 29 cm/s. White dashed line is summit of seamount. Black line shows hydrophone RMS amplitude overlain on stacked-curtain, showing correspondence between individual eruptive burst and bubble cloud rise.

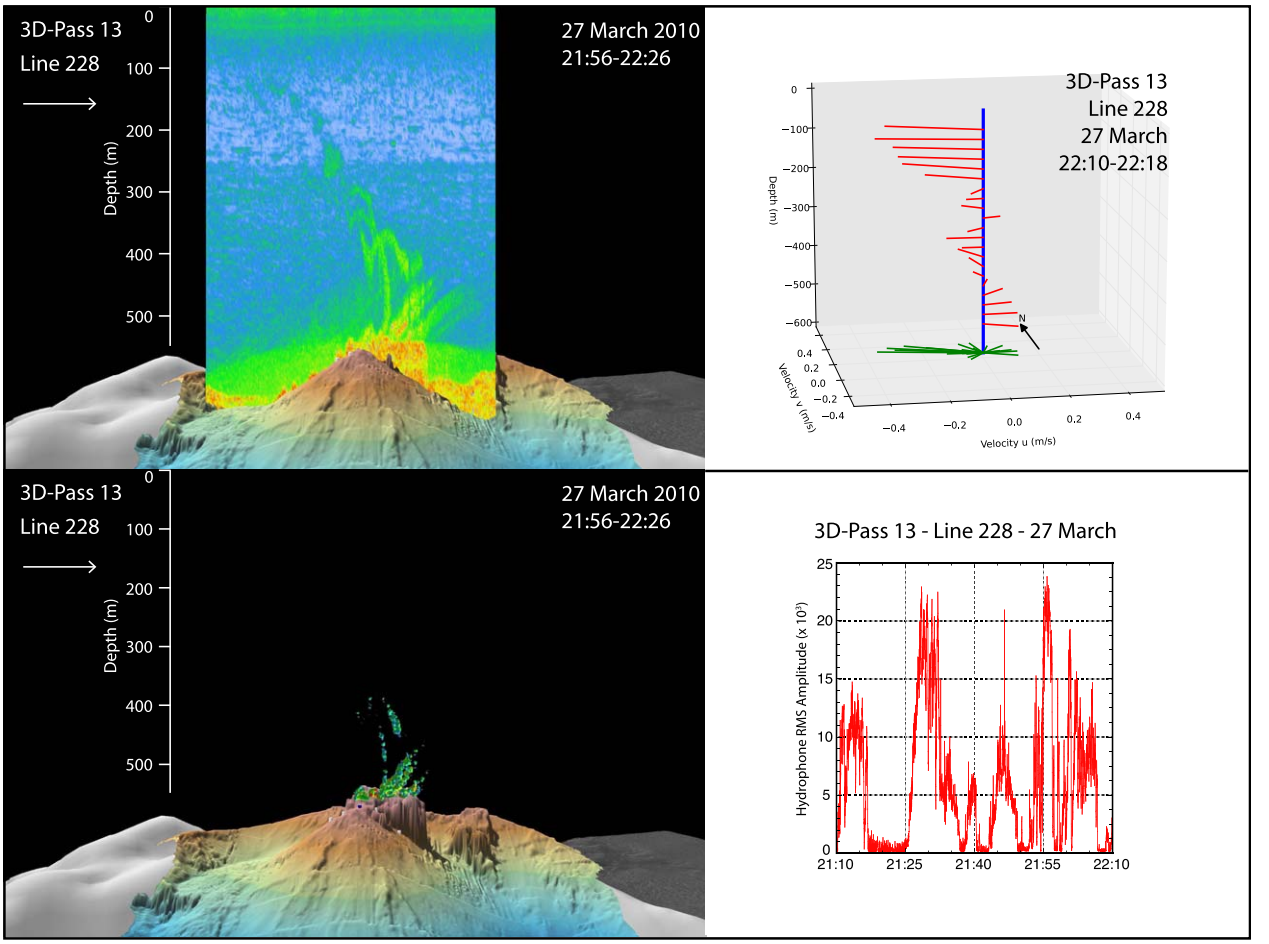

Figure 13. Composite of 2-D stacked-curtain, 3-D volume-object, ADCP data, and hydrophone RMS amplitude for 3-D-pass 13, allowing easier comparison of multibeam data, with ocean currents and eruptive activity. Note currents are westward at shallow depths and eastward below ~300 m, which is reflected in the increased shear and disruption of the bubble plume in the multibeam data. Movie 10 is a time-lapse movie of similar composite plots for the entire 3-D-pass time series.

Our results show that the bubble plumes at NW Rota-1 are essentially independent from the hydrothermal plume, even though they are emitted from the same source. ROV observations show that the CO_2 bubbles separate from the hydrothermal plume within a few meters of the vent because of their greater buoyancy. Previous CTD data show that the top of hydrothermal plumes at NW Rota-1 are typically between 450 and 520 m depth, corresponding to a rise height of 75 and 100 m [*Resing et al*., 2007; *Baker et al*., 2008; *Walker et al*., 2008]. At that depth, the hydrothermal plume loses its buoyancy and spreads laterally due to mixing with ambient seawater and a steepening of the local vertical density gradient at ~480 m depth. In contrast, the bubble plumes in the multibeam data rose well above the hydrothermal plume reaching depths between 150 and 350 m (Figure 5 and Movie 5).

The rise height of the bubble plumes in the multibeam data reflects the limit at which they are acoustically detectable; the actual bubbles may rise somewhat higher. As the bubbles rise, they gradually decrease in size as the CO_2 dissolves into the surrounding ocean [*Leifer and Patro*, 2002; I. Leifer, personal communication, 2014]. The EM122 multibeam sonar can likely sense the CO_2 bubbles at NW Rota-1 until they fall below ~1–2 mm in diameter, because the theoretical acoustic target strength of bubbles (at these depths, with 12 kHz sonar) is relatively high until they shrink below that size [*Weber et al*., 2014; T. Weber, personal communication, 2014]. The number and spatial density of bubbles is also an important factor in whether or not they are detected when insonified. There is some evidence from the multibeam data that the higher ocean currents at shallower depths (Figure 7 and Movie 7) act to break up the coherency of the bubble plumes above ~300 m. For example, in Figure 5 and Movie 5, the tops of bubble plumes that rise above 300 m tend to be disconnected from the lower plume stem and more convoluted in shape, suggesting that

increased current shear acts to disrupt and disperse the plume tops above that depth. This is also shown in Figure 13 and Movie 10. Likewise, the bubble plumes often have a distinct inflection toward the down-current direction, often above a depth of ~400 m (Figure 5 and Movie 5), likely caused by the higher current velocities at shallower depths, as seen in the ADCP data (Figure 7 and Movie 7).

The sonar data also reflect the difference in the behavior of the two eruptive vents on the seafloor. In Figure 5 and Movie 5, the bubble plume from Sulfur vent (at left) is consistently more vertically continuous and lower in acoustic amplitude, a product of the continuous emission of bubbles at a relatively low flux from that vent. In contrast, the bubble plume from Styx vent (at right) tends to be made up of "puffs" or groups of coherent bubble clouds separated from one another that tend to be higher in acoustic amplitude. This puffing is likely caused by the intermittent eruptive bursts at Styx vent, cycling between very high flux and no flux every few minutes when the vent was active.

The variation of the maximum plume height with time in the multibeam 3-D-pass time series is likely due to variation of (1) the maximum size of bubbles expelled during explosive bursts (larger bursts create larger bubbles), (2) the number of bubbles emitted during explosive bursts, which could induce enhanced upward convection due to a reduction of the average fluid density when many bubbles are present, and (3) the interaction of the bubble plumes with the variable ocean current, which may act to preserve or disrupt their coherency as they rise, depending on current shear.

Our main conclusions are the following:

1. At NW Rota-1, plumes of CO_2 bubbles are distinct from sulfur-rich hydrothermal plumes, which only rise $<$100 m above the vents before becoming neutrally buoyant and spreading laterally. CO_2 bubble plumes in the midwater multibeam data typically rise 200–300 m (but sometimes up to 400 m) above the vent before they dissipate.

2. CO_2 bubble plumes were imaged above the volcano on every multibeam sonar pass during the 19 h 3-D-pass time series, but they varied in size and amplitude with eruptive activity, and their orientation was consistent with ocean currents at the time.

3. CO_2 output on the seafloor during the time series was from two distinct eruptive vents—one continuous and passive (Sulfur vent), the other cyclic and explosive (Styx vent). The two sources, located 55 m apart, produced two separate bubble plumes that were distinguishable in the multibeam data. The one from Sulfur was lower amplitude, vertically continuous, and connected to the seafloor, whereas the one from Styx was higher amplitude, and vertically discontinuous, reflecting the differences in degassing styles at the vents.

4. The deflection direction and distance of the multibeam 3-D volume-objects correlate strongly with the ocean current direction and velocity determined from ADCP data.

5. The height, amplitude, and volume of the 3-D volume-objects correlate with the maximum hydrophone RMS amplitude or the percent of the time the Styx eruptive vent was active in the previous hour.

6. Thus, multibeam midwater sonar data can provide valuable, remotely collected information on the location, intensity, and temporal variability of eruptive activity on the seafloor at an active submarine volcano.

Future work at NW Rota-1 will compare multibeam midwater data to more quantitative measures of CO_2 flux, including CTD-based measurement of water chemistry over the volcano, and recently developed hydroacoustic methods of estimating gas flux [*Dziak et al.*, 2012].

Acknowledgments

This paper benefited from helpful reviews by Tom Weber and two anonymous reviewers. We thank the captain and crew of the *R/V Kilo Moana* and the *Jason* ROV team for their excellent support at sea during the 2010 expedition to NW Rota-1 (KM1005). Robert Embley participated in the 2010 expedition and contributed to the geologic interpretations of eruptive activity at NW Rota-1. Help and advice from Moe Doucet at Fledermaus and Mark Amend at Kongsberg is greatly appreciated. Ira Leifer generously provided valuable guidance and feedback regarding bubble plume behavior and modeling and made helpful comments on an earlier version of the manuscript. The midwater multibeam sonar data and hydrophone data presented in this paper are available by request from William Chadwick (william.w.chadwick@noaa.gov). Other data are available at the Marine Geoscience Data System (www.marine-geo.org), the Joint Archive for Shipboard ADCP (ilikai.soest.hawaii.edu/sadcp/), and the National Deep Submergence Facility archive at WHOI (www.whoi.edu/main/ndsf/data). Support for this study was provided by NSF grants OCE-0751776 and OCE-1233717. This is PMEL contribution 4209.

References

Baker, E. T., R. W. Embley, S. L. Walker, J. A. Resing, J. E. Lupton, K. Nakamura, C. E. J. de Ronde, and G. J. Massoth (2008), Hydrothermal activity and volcano distributions along the Mariana Arc, *J. Geophys. Res.*, *113*, B08S09, doi:10.1029/2007JB005423.

Butterfield, D. A., K. Nakamura, B. Takano, M. D. Lilley, J. E. Lupton, J. A. Resing, and K. K. Roe (2011), High SO_2 flux, sulfur accumulation and gas fractionation at an erupting submarine volcano, *Geology*, *39*(9), 803–806, doi:10.1130/G31901.1.

Cardigos, F., A. Colaço, P. R. Dando, S. P. Ávila, P.-M. Sarradin, F. Tempera, P. Concieção, A. Pascoal, and R. Serrão Santos (2005), Shallow water hydrothermal vent field fluids and communities of the D. João de Castro Seamount (Azores), *Chem. Geol.*, *224*, 153–168, doi:10.1016/j.chemgeo.2005.07.019.

Caudron, C., A. Mazot, and A. Bernard (2012), Carbon dioxide dynamics in Kelud volcanic lake, *J. Geophys. Res.*, *117*, B05102, doi:10.1029/2011JB008806.

Chadwick, W. W., Jr., K. V. Cashman, R. W. Embley, H. Matsumoto, R. P. Dziak, C. E. J. de Ronde, T.-K. Lau, N. Deardorff, and S. G. Merle (2008), Direct video and hydrophone observations of submarine explosive eruptions at NW Rota-1 Volcano, Mariana Arc, *J. Geophys. Res.*, *113*, B08S10, doi:10.1029/2007JB005215.

Chadwick, W. W., Jr., R. P. Dziak, J. H. Haxel, R. W. Embley, and H. Matsumoto (2012), Submarine landslide triggered by volcanic eruption recorded by in-situ hydrophone, *Geology*, *40*(1), 51–54, doi:10.1130/G32495.1.

de Ronde, C. E. J., et al. (2005), Evolution of a submarine magmatic-hydrothermal system: Brothers volcano, southern Kermadec arc, New Zealand, *Econ. Geol.*, *100*, 1097–1133.

Deardorff, N. D., K. V. Cashman, and W. W. Chadwick Jr. (2011), Observations of eruptive plumes and pyroclastic deposits from submarine explosive eruptions at NW Rota-1, Mariana Arc, *J. Volcanol. Geotherm. Res.*, *202*(1-2), 47–59, doi:10.1016/j.jvolgeores.2011.01.003.

Dziak, R. P., E. T. Baker, A. M. Shaw, D. R. Bohnenstiehl, W. W. Chadwick Jr., J. H. Haxel, H. Matsumoto, and S. L. Walker (2012), Flux measurements of explosive degassing using a year-long hydroacoustic record at an erupting submarine volcano, *Geochem. Geophys. Geosyst.*, *13*, Q0AF07, doi:10.1029/2012GC004211.

Embley, R. W., et al. (2006), Long-term eruptive activity at a submarine arc volcano, *Nature*, *441*, 494–497, doi:10.1038/nature04762.

Firing, E., and J. M. Hummon (2010), Shipboard ADCP measurements, in *The GO-SHIP Repeat Hydrography Manual: A Collection of Expert Reports and Guidelines, IOCCP Rep. 14, ICPO Publ. Ser.*, vol. 134. [Available at http://www.go-ship.org/HydroMan.html.]

Firing, E., J. M. Hummon, and T. K. Chereskin (2012), Improving the quality and accessibility of current profile measurements in the Southern Ocean, *Oceanography*, *25*(3), 164–165, doi:10.5670/oceanog.2012.91.

Gardner, J. V. (2009), Plume 1400 meters high discovered at the seafloor off the northern California margin, *Eos Trans. AGU*, *90*, 275.

Greinert, J. (2008), Monitoring temporal variability of bubble release at seeps: The hydroacoustic swath system GasQuant, *J. Geophys. Res.*, *113*, C07048, doi:10.1029/2007JC004704.

Greinert, J., Y. Artemov, V. Egorov, M. De Batist, and D. McGinnis (2006), 1300-m-high rising bubbles from mud volcanoes at 2080m in the Black Sea: Hydroacoustic characteristics and temporal variability, *Earth Planet. Sci. Lett.*, *244*, 1–15, doi:10.1016/j.epsl.2006.02.011.

Greinert, J., D. F. McGinnis, L. Naudts, P. Linke, and M. De Batist (2010), Atmospheric methane flux from bubbling seeps: Spatially extrapolated quantification from a Black Sea shelf area, *J. Geophys. Res.*, *115*, C01002, doi:10.1029/2009JC005381.

Hughes-Clarke, J. E. (2009), Repetitive surface-mounted multibeam water column imaging of hydrothermal vent plumes over NW Rota 1, *Eos Trans. AGU*, *90*(52), Fall Meet. Suppl., Abstract V51D-1716.

Kannberg, P. K., A. M. Trehu, S. D. Pierce, C. K. Paull, and D. W. Caress (2013), Temporal variation of methane flares in the ocean above Hydrate Ridge, Oregon, *Earth Planet. Sci. Lett.*, *368*, 33–42, doi:10.1016/j.epsl.2013.02.030.

Leifer, I., and R. K. Patro (2002), The bubble mechanism for methane transport from the shallow sea bed to the surface: A review and sensitivity study, *Cont. Shelf Res.*, *22*, 2409–2428.

Leifer, I., M. J. Kamerling, B. P. Luyendyk, and D. S. Wilson (2010), Geologic control of natural marine hydrocarbon seep emissions, Coal Oil Point seep field, California, *Geo Mar. Lett.*, *30*, 331–338, doi:10.1007/s00367-010-0188-9.

Lupton, J. E., M. Lilley, D. A. Butterfield, L. Evans, R. W. Embley, G. Massoth, B. Christenson, K. Nakamura, and M. Schmidt (2008), Venting of a separate CO_2-rich gas phase from submarine arc volcanoes: Examples from the Mariana and Tonga-Kermadec arcs, *J. Geophys. Res.*, *113*, B08S12, doi:10.1029/2007JB005467.

Medwin, H., and C. S. Clay (1998), *Fundamentals of Acoustical Oceanography*, Academic, Boston, Mass.

Resing, J. A., G. Lebon, E. T. Baker, J. E. Lupton, R. W. Embley, G. J. Massoth, W. W. Chadwick Jr., and C. E. J. de Ronde (2007), Venting of acid-sulfate fluids in a high-sulfidation setting at NW Rota-1 submarine volcano on the Mariana Arc, *Econ. Geol.*, *102*, 1047–1061.

Sauter, E. J., S. I. Muyakshin, J.-L. Charlou, M. Schlüter, A. Boetius, K. Jerosch, E. Damm, J.-P. Foucher, and M. Klages (2006), Methane discharge from a deep-sea submarine mud volcano into the upper water column by gas hydrate-coated methane bubbles, *Earth Planet. Sci. Lett.*, *243*, 354–365, doi:10.1016/j.epsl.2006.01.041.

Schneider von Deimling, J., J. Brockhoff, and J. Greinert (2007), Flare imaging with multibeam systems: Data processing for bubble detection at seeps, *Geochem. Geophys. Geosyst.*, *8*, Q06004, doi:10.1029/2007GC001577.

Schneider von Deimling, J., J. Greinert, N. R. Chapman, W. Rabbel, and P. Linke (2010), Acoustic imaging of natural gas seepage in the North Sea: Sensing bubbles controlled by variable currents, *Limnol. Oceanogr. Methods*, *8*, 155–171, doi:10.4319/lom.2010.8.155.

Schneider von Deimling, J., G. Rehder, J. Greinert, D. F. McGinnis, A. Boetius, and P. Linke (2011), Quantification of seep-related methane gas emissions at Tommeliten, North Sea, *Cont. Shelf Res.*, *31*(7-8), 867–878, doi:10.1016/j.csr.2011.02.012.

Walker, S. L., E. T. Baker, J. A. Resing, W. W. Chadwick Jr., G. T. Lebon, J. E. Lupton, and S. G. Merle (2008), Eruption-fed particle plumes and volcaniclastic deposits at a submarine volcano: NW-Rota-1, Mariana Arc, *J. Geophys. Res.*, *113*, B08S11, doi:10.1029/2007JB005441.

Weber, T. C., L. Mayer, K. Jerram, J. Beaudoin, Y. Rzhanov, and D. A. Lovalvo (2014), Acoustic estimates of methane gas flux from the seabed in a 6000 km^2 region in the Northern Gulf of Mexico, *Geochem. Geophys. Geosyst.*, *15*, 1911–1925, doi:10.1002/2014GC005271.

Westbrook, G. K., et al. (2009), Escape of methane gas from the seabed along the West Spitsbergen continental margin, *Geophys. Res. Lett.*, *36*, L15608, doi:10.1029/2009GL039191.